Single-atom Pt boosting electrochemical non-enzymatic glucose sensing on $Ni(OH)_2$/N-doped graphene

Baojun Long[1#], Yuanmeng Zhao[1#], Peiyu Cao[1], Wen Wei[1], Yan Mo[1], Juejing Liu[3], Cheng-Jun Sun[4], Xiaofeng Guo[3]*, Changsheng Shan[1]*, Ming-Hua Zeng[1, 2]*

[1]Ministry-of-Education Key Laboratory for the Synthesis and Application of Organic Functional Molecules, College of Chemistry and Chemical Engineering, Hubei University, Wuhan, Hubei 430062, P. R. China.

[2]Key Laboratory for the Chemistry and Molecular Engineering of Medicinal Resources, School of Chemistry and Pharmaceutical Sciences, Guangxi Normal University, Guilin, Guangxi, 541004, P.R. China.

[3]Department of Chemistry and Alexandra Navrotsky Institute for Experimental Thermodynamics, Washington State University, Pullman, WA 99164, USA.

[4]X-ray Science Division, Argonne National Laboratory, Argonne, IL 60439, USA.

ABSTRACT: Conventional nanomaterials in electrochemical non-enzymatic sensing face huge challenge due to their complex size-, surface- and composition- dependent catalytic properties and low active site density. In this work, we designed a single-atom Pt supported on $Ni(OH)_2$ nanoplates/nitrogen-doped graphene ($Pt_1/Ni(OH)_2$/NG) as the first example for constructing a single-atom catalyst based electrochemical non-enzymatic glucose sensor. The resulting $Pt_1/Ni(OH)_2$/NG exhibited a low anode peak potential of 0.48 V and high sensitivity of 220.75 μA mM^{-1} cm^{-2} towards glucose, which are 45 mV lower and 12 times higher than those of $Ni(OH)_2$, respectively. The catalyst also showed excellent selectivity for several important interferences, short response time of 4.6 s, and high stability over 4 weeks. Experimental and density functional theory (DFT) calculated results reveal that the improved performance of $Pt_1/Ni(OH)_2$/NG could be attributed to stronger binding strength of glucose on single-atom Pt active centers and their surrounding Ni atoms, combined with fast electron transfer ability by the adding of the highly conductive NG. This research sheds light on the applications of SACs in the field of electrochemical non-enzymatic sensing.

Diabetes is a serious metabolic disease with a long-term high glucose concentration in blood,[1,2] which can cause serious complications, such as kidney failure, blindness and heart disease.[3-5] It is required to develop highly effective sensors for the quick and accurate monitoring for glucose. A common method for glucose detecting is electrochemical enzymatic biosensing, which is susceptible to external environments (pH and temperature) due to the instability of enzymes.[6,7] Therefore, non-enzymatic nanomaterial-based electrochemical sensors, such as metals,[8,9] metal oxides,[10,11] and hydroxide,[12,13] were developed extensively. However, the poor catalytic activity and selectivity of most nanomaterials limited their practical applications. More importantly, it is very difficult to investigate the catalytic sites at the atomic scale and understand the characteristics of the catalysts due to the complex structures and compositions of nanomaterials.[14,15] Therefore, highly effective electrocatalysts with well-defined active centers are critically required for developing new generation of electrochemical non-enzymatic glucose sensors.[16,17]

Single-atom catalysts have metal atoms dispersed on solid supports as well-defined catalytic active centers.[18,19] The well-defined catalytic active sites have enabled the clarification of the relationship between catalytic performance and the active site structure.[20,21] However, the cooperative catalytic effect between the single atoms and the supports is often overlooked. In addition, the SACs with high activity and 100% utilization of metal atoms are promising for a variety of catalytic applications,[22-25] especially in electrocatalysis.[26-33] However, there are seldom reports about SACs in electrochemical biosensing,[20,34] especially no study about electrochemical non-enzymatic glucose sensing to our best knowledge.

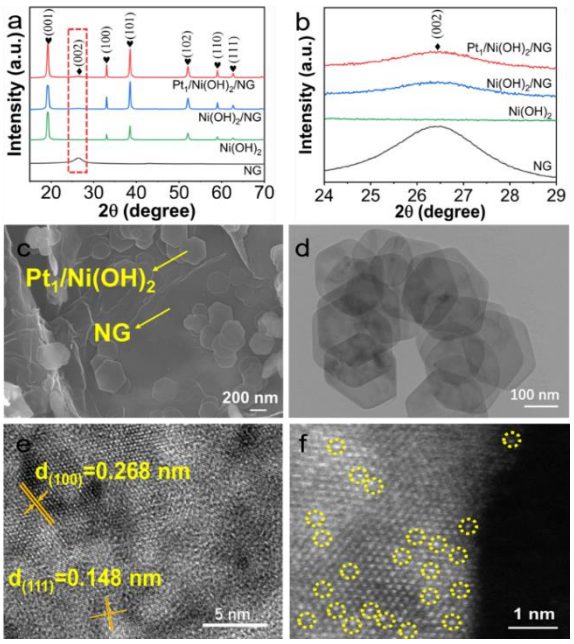

Figure 1. XRD patterns (a) and enlarged XRD patterns (b, from red dashed frame area in Figure 1a) of NG, $Ni(OH)_2$, $Ni(OH)_2$ /NG, $Pt_1/Ni(OH)_2$/NG; ♥ and ♦ represent the characteristic peaks of $Ni(OH)_2$ and NG, respectively. SEM (c), TEM (d), HRTEM (e) and AC-HAADF-STEM (f) images of $Pt_1/Ni(OH)_2$/NG.

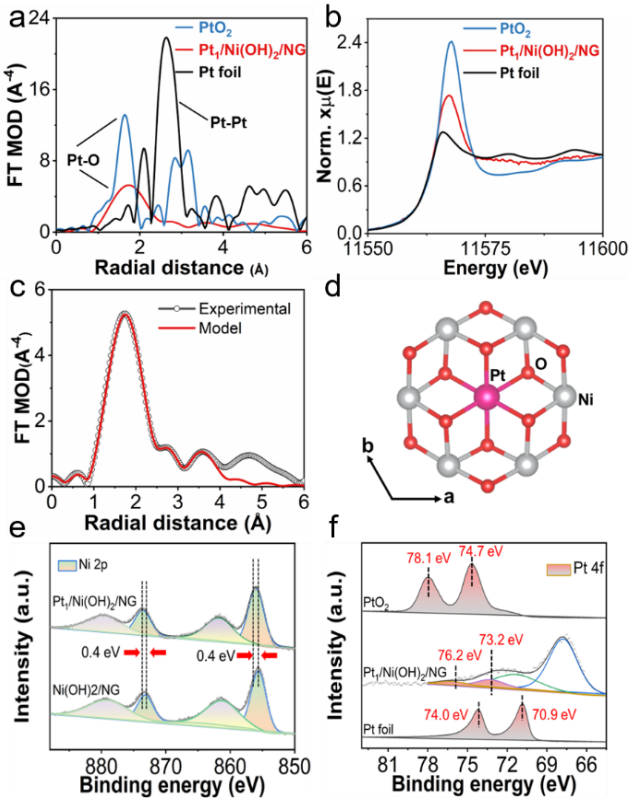

Figure 2. The FT-EXAFS spectra of (a) and XANES spectra (b) of $Pt_1/Ni(OH)_2$/NG, PtO_2, and Pt foil at Pt L_{III}-edge. (c) The FT-EXAFS curves between the experimental and fitted data. (d) Schematic illustration of the Pt single atom replacing a Ni atom in $Ni(OH)_2$/NG. High-resolution XPS spectra of Ni 2p region (e) and Pt 4f region (f).

In order to develop the SACs in electrochemical non-enzymatic glucose sensing and understand the cooperative catalytic mechanism between single atoms and their supporters, the $Pt_1/Ni(OH)_2$/NG is designed for electrochemical non-enzymatic glucose sensing in this work. The Pt single atoms were confirmed by aberration-corrected high angle angular dark field-scanning transmission electron microscopy (AC-HAADF-STEM) and extended X-ray absorption fine structure (EXAFS). The $Pt_1/Ni(OH)_2$/NG exhibits high sensitivity of 220.75 μA mM^{-1} cm^{-2}, excellent selectivity, short response time of 4.6 s and high stability in electrochemical non-enzymatic glucose sensing. The cooperative catalytic mechanism between Pt single atoms and the $Ni(OH)_2$/NG is investigated in detail to interpret the superior sensing performance of $Pt_1/Ni(OH)_2$/NG sensor by experimental results and DFT calculations.

The synthetic process of $Pt_1/Ni(OH)_2$/NG is shown in **Figure S1**. First, small $Ni(OH)_2$ nanoparticles are uniformly grown on the NG by hydrolysis of $Ni(Ac)_2$ at 80 °C in a mixed N,N-dimethyl-formamide (DMF)/H_2O solution (**Figure S2a**). Then the $Ni(OH)_2$ nanoparticles gradually evolve into hexagonal $Ni(OH)_2$ nanoplates (**Figure S2b**) under the hydrothermal condition at 180 °C. After that, the $Pt_1/Ni(OH)_2$/NG is finally obtained by adsorption of Pt precursors on $Ni(OH)_2$/NG in ethanol and annealing at 100 °C under 10% H_2/N_2 atmosphere. The loading amount of Pt on $Ni(OH)_2$/NG is 0.36 wt% determined by inductively coupled plasma optical emission spectra (ICP-OES) analysis. The energy dispersive X-ray (EDX) spectroscopy analysis showed 0.32 wt% loading amount of Pt in $Pt_1/Ni(OH)_2$/NG, similar with ICP-OES result (**Figure S3**).

The $Pt_1/Ni(OH)_2$/NG is first characterized by X-ray diffraction (XRD). As observed in **Figure 1a**, it displays characteristic diffraction peaks at 19.6°, 33.4°, 38.8°, 52.2°, 59.2° and 62.7 °, which are indexed to (001), (100), (101), (102) and (111) planes of the $Ni(OH)_2$ phase (JCPDS No. 03-0177),[35] respectively. The peak at 26.4° corresponds to the (002) plane of NG (**Figure 1b**).[35] No characteristic peaks of Pt are detected, implying the absence of Pt nanoparticles. As shown in **Figure 1c** and **Figure S4a**, the hexagonal $Pt_1/Ni(OH)_2$ nanoplates are observed and show no obvious change compared to $Ni(OH)_2$/NG and pure $Ni(OH)_2$ (**Figure S4b-c**). The average side length of hexagonal $Ni(OH)_2$ nanoplates in $Pt_1/Ni(OH)_2$/NG is ca. 183 nm. The mapping images of EDX show the homogeneous distributions of C, N, O, Ni and Pt elements in $Pt_1/Ni(OH)_2$/NG (**Figure S5**).

Transmission electron microscopy (TEM) is conducted to further investigate the morphology and structure of $Pt_1/Ni(OH)_2$/NG. A hexagonal morphology of $Ni(OH)_2$ nanoplates in $Pt_1/Ni(OH)_2$/NG is observed in **Figure 1d**,

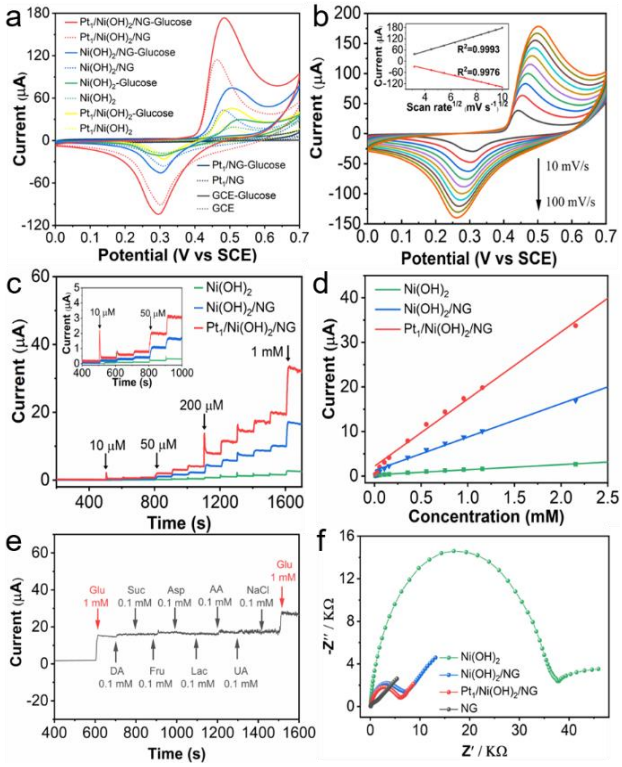

Figure 3. (a) The CV curves of GEC (grey), Pt_1/NG (navy blue), $Ni(OH)_2$ (green), $Pt_1/Ni(OH)_2$ (light blue), $Ni(OH)_2$/NG (blue), $Pt_1/Ni(OH)_2$/NG (red) at a scan rate of 50 mV/s in 0.1 M NaOH with the absence (dotted line) and presence (solid line) of 1 mM glucose. (b) CV curves for $Pt_1/Ni(OH)_2$/NG in 0.1 M NaOH at different scan rates from 10 to 100 mV/s and (inset: the corresponding plots of current density vs the square root of scan rate). (c) (c) Amperometric responses of Ni(OH)2, Ni(OH)2/NG, Pt1/Ni(OH)2/NG in 0.1 M NaOH at 0.5 V. (inset: the enlarged plot in the range from 400 to 1000 s). (d) the corresponding calibration curve of current response vs glucose concentration. (e) Amperometric responses of $Pt_1/Ni(OH)_2$/NG with the successive addition of 1 mM glucose, 0.1 mM DA, 0.1 mM Suc, 0.1 mM Fru, 0.1 mM Asp, 0.1 mM Lac, 0.1 mM AA, 0.1 mM UA, 0.1 mM NaCl and 1 mM glucose at 0.5 V in 0.1 M NaOH.

which is consistent with SEM images. And the lattice fringe spacings of 0.268 and 0.148 nm correspond to the (100) and (111) planes of $Ni(OH)_2$ in high-resolution TEM (HRTEM) image in **Figure 1e**, respectively. The AC-HAADF-STEM was used for studying the dispersibility of Pt atoms on the $Ni(OH)_2$/NG. The bright spots in **Figure 1f** are corresponding to the isolated Pt atoms on $Ni(OH)_2$/NG without the observation of Pt clusters or nanoparticles, indicating successful synthesis of Pt single atoms.

The existence of Pt single atoms is further confirmed by X-ray absorption spectroscopy. The fourier-transform EXAFS (FT-EXAFS) spectra of $Pt_1/Ni(OH)_2$/NG show one main peak located at ~1.6 Å, attributing to the Pt-O path and sharply contrasting with that to the Pt-Pt bonds (~2.6 Å) in the spectra of Pt foil or PtO_2 (**Figure 2a**). This result clearly indicates the existence of Pt single atoms in $Pt_1/Ni(OH)_2$/NG. The valence state of the Pt single atoms is determined by the linear combination fitting of its X-ray absorption near-edge structure (XANES) spectrum (**Figure 2b**) using XANES spectra of PtO_2 and Pt foil. As shown in **Figure 2b**, the peak intensity of $Pt_1/Ni(OH)_2$/NG is between PtO_2 (valence: +4) and Pt foil (valence: 0). The valence state of Pt in $Pt_1/Ni(OH)_2$/NG is estimated to be about +1.6 (**Figure S6**). Moreover, EXAFS fitted by the theoretical scattering patterns (**Figure 2c and Table S1**) shows that each Pt atom is coordinated with 6.9 ± 0.7 oxygen atoms, while Ni atom is coordinated with 6.0 ± 0.8 oxygen atoms, similar to the coordination number of Pt here. This strongly suggests that each Pt atom substitutes a Ni atom in $Ni(OH)_2$/NG in isolated single atomic sites (**Figure 2d**).

The XPS is used to study the electronic interaction between Pt and Ni. In **Figure 2e**, the binding energies of Ni $2p_{3/2}$ and $2p_{1/2}$ of $Pt_1/Ni(OH)_2$/NG exhibit 0.4 eV higher than those of pristine $Ni(OH)_2$/NG after the introduction of Pt, indicating the higher valence state of Ni in $Pt_1/Ni(OH)_2$/NG.[36] This can be attributed to the incorporation of Pt single atoms with lower valence state (+1.6 valence from XANES).[37] Additionally, the 4f peaks of Pt shift positively compared to the standard Pt and negatively compared to the standard PtO_2 (**Figure 2f**). This confirms that the valence state of Pt in $Pt_1/Ni(OH)_2$/NG is between the valence of 0 and +4, in well agreement with the XANES results. Besides the peaks of Pt_{4f} in **Figure 2f**, the two strong peaks at 67.8 and 71.5 eV are corresponding to the peak of Ni_{3p} and its satellite peak, respectively.[38]

Cyclic voltammetry (CV) is used to study the electrochemical behaviors of $Pt_1/Ni(OH)_2$/NG towards electrochemical glucose sensing. **Figure 3a** shows the current responses of different electrodes in the presence or absence of glucose at a scan rate of 50 mV/s. The glassy carbon electrode (GCE) and Pt_1/NG do not show any redox peak. And other catalysts show a pair of redox peaks, which are caused by the redox pair of Ni(II)/Ni(III) in alkaline medium.[39] The oxidation peak potential of Ni(II)/Ni(III) in $Pt_1/Ni(OH)_2$/NG is 0.460 V, much lower than those of $Ni(OH)_2$/NG (0.485 V), $Pt_1/Ni(OH)2$ (0.489 V) and $Ni(OH)_2$ (0.513 V). After the addition of 1 mM glucose, the GCE shows no oxidation activity for glucose, while the Pt_1/NG shows a weak oxidation current for glucose without oxidation peak (**Figure S7**). And the anodic peak potential of $Pt_1/Ni(OH)_2$/NG is 0.480 V, lower than those of $Ni(OH)_2$/NG (0.506 V), $Pt_1/Ni(OH)_2$ (0.505 V) and $Ni(OH)_2$ (0.525 V). Meantime, $Pt_1/Ni(OH)_2$/NG exhibits the highest anodic peak current (174 μA), 2.35, 3.79 and 6.21-folds higher than those of the $Ni(OH)_2$/NG (74 μA), $Pt_1/Ni(OH)_2$ (45.9 μA) and $Ni(OH)_2$ (28 μA), respectively. As a control, the Pt nanoparticles (PtNPs) on Ni(OH)2/NG (0.49 wt%, ICP-OES analysis) were also synthesized for electrochemical oxidation of glucose (**Figure S8 and Figure S9**). From cyclic voltammetry in **Figure 3a** and **Figure S9**, the Pt1/Ni(OH)2/NG exhibited much lower oxidation potential (0.480 V) to glucose than those of PtNPs/Ni(OH)2/NG (0.521 V). These results show that the

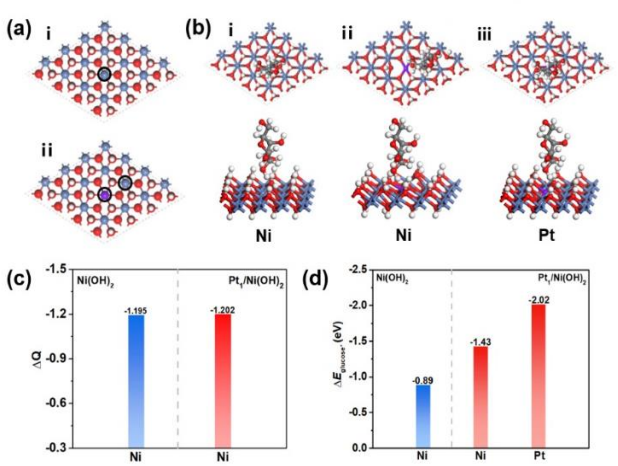

Figure 4. (a) The structural models of $Ni(OH)_2$ (i) and $Pt_1/Ni(OH)_2$ (ii). (b) The optimized structure models of the adopted glucose adsorption sites of $Ni(OH)_2$ (i) and $Pt_1/Ni(OH)_2$ (ii and iii). The light blue, purple, gray, red and white balls represent Ni, Pt, C, O, and H atoms, respectively. (c) The Bader charge analysis. ΔQ = Q (Ni in $Ni(OH)_2$ or $Pt_1/Ni(OH)_2$) - Q (the number of valence electrons for Ni), Q is the calculated Bader electron number of Ni atoms. The negative value in ΔQ represents the number of electron loss of the atoms. (d) The corresponding binding energies of glucose on $Ni(OH)_2$ and $Pt_1/Ni(OH)_2$.

adding of single-atom Pt and high conductivity of NG could promote the electrochemical oxidation of Ni(II) to Ni(III)OOH, which results in the high electrocatalytic activity of $Pt_1/Ni(OH)_2$/NG towards glucose with lower oxidation potential and higher current response.[40] To further study the electrochemical behavior of $Pt_1/Ni(OH)_2$/NG, the cyclic voltammograms of $Pt_1/Ni(OH)_2$/NG modified electrode at various scan rates (10 ~ 100 mV/s) were investigated (**Figure 3b**). In **Figure 3b** inset, a good linear relationship between peak current and the square root of scan rates can be observed, suggesting that the redox reaction on the electrode is a typical surface diffusion control.[41]

On the basis of the high electrocatalytic activity of $Pt_1/Ni(OH)_2$/NG towards glucose, a SACs sensor based on $Pt_1/Ni(OH)_2$/NG is developed for amperometric detecting of glucose. The amperometric response of $Pt_1/Ni(OH)_2$/NG modified electrode with the successive addition of glucose is conducted at an applied potential of 0.5 V in 0.1 M NaOH shown in **Figure 3c**. The anodic current of $Pt_1/Ni(OH)_2$/NG increases linearly with glucose concentration over the range from 0.01 mM to 2.18 mM with best linearity (R^2=0.992) and the highest sensitivity (220.75 μA mM^{-1} cm^{-2}) compared to $Ni(OH)_2$/NG (R^2 of 0.989, 110.47 μA mM^{-1} cm^{-2}) and $Ni(OH)_2$ (R^2 of 0.980 and the sensitivity of 17.13 μA mM^{-1} cm^{-2}) in **Figure 3d**. In addition, $Pt_1/Ni(OH)_2$/NG shows a faster response time of ca. 4.6 s than $Ni(OH)_2$/NG (ca. 7.1 s) and $Ni(OH)_2$ (ca. 9.3 s) in **Figure S10.**

The selectivity of $Pt_1/Ni(OH)_2$/NG electrochemical sensor is also important for a sensor. Various inorganic and organic substances, such as dopamine (DA), sucrose (Suc), fructose (Fru), aspartic acid (Asp), lactose (Lac), ascorbic acid (AA), uric acid (UA), NaCl, coexist with glucose in the blood, which seriously interferes with the determination of glucose.[42,43] **Figure 3e** shows amperometric responses of $Pt_1/Ni(OH)_2$/NG at 0.50 V in 0.1 M NaOH with successive addition of 1 mM glucose and 0.1 mM various interfering species. The $Pt_1/Ni(OH)_2$/NG shows a remarkable current response to glucose with negligible response to these interfering species, and meantime keeps great current response in the presence of these interfering species. These results demonstrate the excellent selectivity of $Pt_1/Ni(OH)_2$/NG for glucose sensing. Further, the stability of $Pt_1/Ni(OH)_2$/NG sensor was also examined. The amperometric response towards glucose only decreases by 2.15% after 28 days (**Figure S11**), indicating the outstanding long-term stability of $Pt_1/Ni(OH)_2$/NG sensor. In addition, the morphology of Pt1/Ni(OH)2/NG is still kept well with hexagon nanoplates of Pt1/Ni(OH)2 without formation of Pt nanoparticles, indicating the excellent structural stability of the catalyst (**Figure S12**). It is worth noting that the $Pt_1/Ni(OH)_2$/NG shows the superior performance compared to most of the reported nanomaterials-based sensors in terms of selectivity, sensitivity, and long-term stability (**Table S2**).

Electrochemical impedance spectroscopy (EIS) is carried out to further understand the intrinsic activities of $Pt_1/Ni(OH)_2$/NG, $Ni(OH)_2$/NG and $Ni(OH)_2$ (**Figure 3f**). The charge transfer resistances (R_{ct}) of $Pt_1/Ni(OH)_2$/NG (5.9 KΩ) and $Ni(OH)_2$/NG (7.0 KΩ) are much lower than that of $Ni(OH)_2$ (37.1 KΩ). This indicates that the improved conductivity of $Pt_1/Ni(OH)_2$/NG is mainly attributed to the adding of highly conductive NG, which can facilitate the electron transfer ability of $Pt_1/Ni(OH)_2$/NG, and promote the electrochemically sensing performance towards glucose.

To achieve a deeper understanding of the electrocatalytic mechanism of $Pt_1/Ni(OH)_2$/NG towards glucose, density functional theory (DFT) calculations are performed. The theoretical models of $Ni(OH)_2$ and $Pt_1/Ni(OH)_2$ are presented in **Figure 4a**, the latter of which is built by replacing one Ni atom in $Ni(OH)_2$ with a Pt atom (**Figure 4a-ii**). The Bader charge analysis (**Figure 4c**) points out that the Ni atoms surround the Pt single atom lose more electrons (1.202) than those in pristine $Ni(OH)_2$ (1.195), suggesting more positive charge on Ni atoms induced by Pt single atom. This result agrees well with the XPS analysis, indicating the strong electronic interactions between single-atom Pt and $Ni(OH)_2$. The binding energies of glucose molecule ($\Delta E_{glucose^*}$) on $Ni(OH)_2$ and $Pt_1/Ni(OH)_2$ surface are also calculated. As shown in **Figure 4b and 4d**, the optimal adsorption site of glucose for $Ni(OH)_2$ is on the Ni site with the binding energy of -0.89 eV, while the most stable adsorption site of glucose for $Pt_1/Ni(OH)_2$ is on the Pt site with the binding energy of -2.02 eV. The much stronger glucose adsorption strength on single-atom Pt indicates that the Pt single atoms are the active centers to greatly enhance catalytic activity of $Pt_1/Ni(OH)_2$/NG for glucose oxidation reaction.[44,45]

Besides, the Ni sites surrounding Pt single atom in $Pt_1/Ni(OH)_2$ also exhibit stronger binding energy of glucose (-1.43 eV) than those in pristine $Ni(OH)_2$. Combining experimental and DFT calculation results, it can be concluded that the Pt single atom not only acts as an important active center for adsorption of glucose, but also actives the surrounding Ni atoms for enhancing the electrochemical non-enzymatic glucose catalysis and sensing. Therefore, the high activity of Pt1/Ni(OH)2/NG for glucose oxidation can be attributed to the synergistic catalytic effect of Pt single atoms, Ni(OH)2 and NG.

In summary, the $Pt_1/Ni(OH)_2$/NG SACs have been successfully fabricated. The Pt single atoms anchored on the $Ni(OH)_2$/NG and their strong electronic interactions with $Ni(OH)_2$ are confirmed by EXAFS, AC-HAADF-STEM and XPS. The resulting $Pt_1/Ni(OH)_2$/NG shows much better performance than $Ni(OH)_2$ towards electrochemical non-enzymatic glucose sensing with high sensitivity (220.75 μA mM^{-1} cm^{-2}), outstanding selectivity for eight interferences (DA, sucrose, fructose, aspartic acid, lactose, AA, UA and NaCl), fast response (ca. 4.6 s) and excellent long-term stability (only 2.15% current decrease after 28 days). From experimental results and DFT calculations, the superior sensing performance of $Pt_1/Ni(OH)_2$/NG is mainly attributed to the synergistic catalytic effect of Pt single aotms and their surrounding Ni atoms. Moreover, the highly conductive NG is also greatly helpful to improve the sensing performance by enhancing the electron transfer ability of $Pt_1/Ni(OH)_2$/NG. To the best of our knowledge, the $Pt_1/Ni(OH)_2$/NG is the first example of SACs for constructing electrochemical non-enzymatic glucose sensing. This work not only presents a vivid example of the cooperative catalytic mechanism between the single atoms and the supporters in the catalytic process, but also suggests the potential to develop a new generation of electrochemical biosensor based on SACs in the future.

ASSOCIATED CONTENT

Supporting Information

The Supporting Information is available free of charge on the ACS Publications website.

Experimental section, SEM images, HAADF-STEM image and corresponding EDX mapping, response time, stability test, comparison of sensing performance (PDF)

AUTHOR INFORMATION

Corresponding Author

*E-mail: zmh@mailbox.gxnu.edu.cn; csshan@hubu.edu.cn; x.guo@wsu.edu.

Author Contributions

#These authors contributed equally to this work.

Notes

The authors declare no conflict of interest.

ACKNOWLEDGMENT

Changsheng Shan acknowledges the support from the National Natural Science Foundation of China (No. 21874031) and "Chu-Tian Scholar" Program of Hubei Province. Ming-Hua Zeng thanks the support from the NSFC of China (No. 22171075), Guangxi Province (No. 2017GXNSFDA198040) and the BAGUI talent program (2019AC26001). Xiaofeng Guo acknowledges the support by the institutional funds and New Faculty Seed Grant from ORAP at WSU. This research used resources of the Advanced Photon Source, an Office of Science User Facility operated for the U.S. Department of Energy (DOE) Office of Science by Argonne National Laboratory, and was supported by the U.S. DOE under Contract No. DE-AC02-06CH11357, and the Canadian Light Source and its funding partners.

REFERENCES

(1) Sehit, E.; Altintas, Z., Significance of nanomaterials in electrochemical glucose sensors: An updated review (2016-2020). *Biosens. Bioelectron.* **2020**, *159*, 112165.

(2) Ki, H.; Jang, H.; Oh, J.; Han, G.-R.; Lee, H.; Kim, S.; Kim, M.-G., Simultaneous detection of serum glucose and glycated albumin on a paper-based sensor for acute hyperglycemia and diabetes mellitus. *Anal. Chem.* **2020**, *92*, 11530-11534.

(3) Wang, Q.; Wei, H.; Zhang, Z.; Wang, E.; Dong, S., Nanozyme: an emerging alternative to natural enzyme for biosensing and immunoassay. *TrAC Trends in Anal. Chem.* **2018**, *105*, 218-224.

(4) Wang, J.; Zhang, L.; Qu, Y.; Yang, Y.; Cao, T.; Cao, Y.; Iqbal, A.; Qin, W.; Liu, Y., Long-Wavelength Ratiometric Fluorescent Probe for the Early Diagnosis of Diabetes. *Anal. Chem.* **2021**, *93*, 11461-11469.

(5) Yu, W.; Huang, J.; Lin, M.; Wei, G.; Yang, F.; Tang, Z.; Zeng, F.; Wu, S., Fluorophore-Dapagliflozin Dyad for Detecting Diabetic Liver/Kidney Damages via Fluorescent Imaging and Treating Diabetes via Inhibiting SGLT2. *Anal. Chem.* **2021**, *93*, 4647-4656.

(6) Zhu, C.; Yang, G.; Li, H.; Du, D.; Lin, Y., Electrochemical sensors and biosensors based on nanomaterials and nanostructures. *Anal. Chem.* **2015**, *87*, 230-249.

(7) Oja, S. M.; Feldman, B.; Eshoo, M. W., Method for low nanomolar concentration analyte sensing using electrochemical enzymatic biosensors. *Anal. Chem.* **2018**, *90*, 1536-1541.

(8) Chen, Q.; Zhou, L.; Jiang, W.; Fan, G., Oxygenated functional group-engaged electroless deposition of ligand-free silver nanoparticles on porous carbon for efficient electrochemical non-enzymatic H2O2 detection. *Nanoscale* **2020**, *12*, 24495-24502.

(9) Kou, B.-B.; Chai, Y.-Q.; Yuan, Y.-L.; Yuan, R., PtNPs as scaffolds to regulate interenzyme distance for construction of efficient enzyme cascade amplification for ultrasensitive electrochemical detection of MMP-2. *Anal. Chem.* **2017**, *89*, 9383-9387.

(10) Yang, P.; Wang, X.; Ge, C.-y.; Fu, X.; Liu, X. Y.; Chai, H.; Guo, X.; Yao, H.-C.; Zhang, Y. X.; Chen, K., Fabrication of CuO nanosheets-built microtubes via Kirkendall effect for non-enzymatic glucose sensor. *Appl. Surf. Sci.* **2019**, *494*, 484-491.

(11) Liu, Y.; Zhao, W.; Li, X.; Liu, J.; Han, Y.; Wu, J.; Zhang, X.; Xu, Y., Hierarchical α-Fe2O3 microcubes supported on Ni foam as non-enzymatic glucose sensor. *Appl. Surf. Sci.* **2020**, *512*, 145710.

(12) Dong, Q.; Yang, L.; He, Z.; Zhang, Y.; Tang, X.; Tang, J.; Huang, K.; Zou, Z.; Xiong, X., Co-Based Transition Metal Hydroxide Nanosheet Arrays on Carbon Cloth for Sensing Glucose and Formaldehyde. *ACS Appl. Nano Mater.* **2021**, *4*, 5076–5083.

(13) Annalakshmi, M.; Kumaravel, S.; Chen, T.-W.; Chen, S.-M.; Lou, B.-S., 3D Flower-like NiCo Layered Double Hydroxides: An Efficient Electrocatalyst for Non-Enzymatic Electrochemical Biosensing of Hydrogen Peroxide in Live Cells and Glucose in Biofluids. *ACS Appl. Bio Mater.* **2021**, *4*, 3203-3213.
(14) Jiao, L.; Yan, H.; Wu, Y.; Gu, W.; Zhu, C.; Du, D.; Lin, Y., When nanozymes meet single - atom catalysis. *Angew. Chem. Int. Ed.* **2020**, *132*, 2585-2596.
(15) Xu, W.; Song, W.; Kang, Y.; Jiao, L.; Wu, Y.; Chen, Y.; Cai, X.; Zheng, L.; Gu, W.; Zhu, C., Axial Ligand-Engineered Single-Atom Catalysts with Boosted Enzyme-Like Activity for Sensitive Immunoassay. *Anal. Chem.* **2021**, *93*, 12758-12766.
(16) Gumilar, G.; Kaneti, Y. V.; Henzie, J.; Chatterjee, S.; Na, J.; Yuliarto, B.; Nugraha, N.; Patah, A.; Bhaumik, A.; Yamauchi, Y., General synthesis of hierarchical sheet/plate-like M-BDC (M= Cu, Mn, Ni, and Zr) metal–organic frameworks for electrochemical non-enzymatic glucose sensing. *Chem. Sci.* **2020**, *11*, 3644-3655.
(17) Wang, A.; Li, J.; Zhang, T., Heterogeneous single-atom catalysis. *Nat. Rev. Chem.* **2018**, *2*, 65-81.
(18) Liu, P.; Zhao, Y.; Qin, R.; Mo, S.; Chen, G.; Gu, L.; Chevrier, D. M.; Zhang, P.; Guo, Q.; Zang, D., Photochemical route for synthesizing atomically dispersed palladium catalysts. *Science* **2016**, *352*, 797-800.
(19) Qiao, B.; Wang, A.; Yang, X.; Allard, L. F.; Jiang, Z.; Cui, Y.; Liu, J.; Li, J.; Zhang, T., Single-atom catalysis of CO oxidation using Pt1/FeOx. *Nat. Chem.* **2011**, *3*, 634-641.
(20) Xie, X.; Wang, D. P.; Guo, C.; Liu, Y.; Rao, Q.; Lou, F.; Li, Q.; Dong, Y.; Li, Q.; Yang, H. B., Single-Atom Ruthenium Biomimetic Enzyme for Simultaneous Electrochemical Detection of Dopamine and Uric Acid. *Anal. Chem.* **2021**, *93*, 4916-4923.
(21) Li, P.-H.; Yang, M.; Li, Y.-X.; Song, Z.-Y.; Liu, J.-H.; Lin, C.-H.; Zeng, J.; Huang, X.-J., Ultra-Sensitive and Selective Detection of Arsenic (III) via Electroanalysis over Cobalt Single-Atom Catalysts. *Anal. Chem.* **2020**, *92*, 6128-6135.
(22) Zhang, H.; Liu, G.; Shi, L.; Ye, J., Single - atom catalysts: emerging multifunctional materials in heterogeneous catalysis. *Adv. Energy Mater.* **2018**, *8*, 1701343.
(23) Li, Z.; Ji, S.; Liu, Y.; Cao, X.; Tian, S.; Chen, Y.; Niu, Z.; Li, Y., Well-defined materials for heterogeneous catalysis: from nanoparticles to isolated single-atom sites. *Chem. Rev.* **2019**, *120*, 623-682.
(24) Wang, Y.; Mao, J.; Meng, X.; Yu, L.; Deng, D.; Bao, X., Catalysis with two-dimensional materials confining single atoms: concept, design, and applications. *Chem. Rev.* **2018**, *119*, 1806-1854.
(25) Liang, Z.; Qu, C.; Xia, D.; Zou, R.; Xu, Q., Atomically dispersed metal sites in MOF - based materials for electrocatalytic and photocatalytic energy conversion. *Angew. Chem. Int. Ed.* **2018**, *57*, 9604-9633.
(26) Li, M.; Duanmu, K.; Wan, C.; Cheng, T.; Zhang, L.; Dai, S.; Chen, W.; Zhao, Z.; Li, P.; Fei, H., Single-atom tailoring of platinum nanocatalysts for high-performance multifunctional electrocatalysis.*Nat. Catal.* **2019**, *2*, 495-503.
(27) Zhang, K.; Wang, H.; Qiu, J.; Wu, J.; Wang, H.; Shao, J.; Deng, Y.; Yan, L., Multi-dimensional Pt/Ni (OH) 2/nitrogen-doped graphene nanocomposites with low platinum content for methanol oxidation reaction with highly catalytic performance. *Chem. Eng. J.* **2020**, 127786.
(28) Luo, E.; Zhang, H.; Wang, X.; Gao, L.; Gong, L.; Zhao, T.; Jin, Z.; Ge, J.; Jiang, Z.; Liu, C., Single - Atom Cr– N_4 Sites Designed for Durable Oxygen Reduction Catalysis in Acid Media. *Angew. Chem.* **2019**, *131*, 12599-12605.
(29) Han, L.; Song, S.; Liu, M.; Yao, S.; Liang, Z.; Cheng, H.; Ren, Z.; Liu, W.; Lin, R.; Qi, G., Stable and efficient single-atom Zn catalyst for CO_2 reduction to CH_4. *J. Am. Chem. Soc.* **2020**, *142*, 12563-12567.
(30) Kobayashi, D.; Kobayashi, H.; Wu, D.; Okazoe, S.; Kusada, K.; Yamamoto, T.; Toriyama, T.; Matsumura, S.; Kawaguchi, S.; Kubota, Y., Significant enhancement of hydrogen evolution reaction activity by negatively charged Pt through light doping of W. *J. Am. Chem. Soc.* **2020**, *142*, 17250-17254.
(31) Liu, W.; Cao, L.; Cheng, W.; Cao, Y.; Liu, X.; Zhang, W.; Mou, X.; Jin, L.; Zheng, X.; Che, W., Single - site active cobalt - based photocatalyst with a Long carrier lifetime for spontaneous overall water splitting. *Angew. Chem.* **2017**, *129*, 9440-9445.
(32) Chen, W.; Pei, J.; He, C. T.; Wan, J.; Ren, H.; Zhu, Y.; Wang, Y.; Dong, J.; Tian, S.; Cheong, W. C., Rational design of single molybdenum atoms anchored on N - doped carbon for effective hydrogen evolution reaction. *Angew. Chem. Int. Ed.* **2017**, *56*, 16086-16090.
(33) Lin, L.; Li, H.; Wang, Y.; Li, H.; Wei, P.; Nan, B.; Si, R.; Wang, G.; Bao, X., Temperature - Dependent CO_2 Electroreduction over Fe - N - C and Ni - N - C Single - Atom Catalysts. *Angew. Chem. Int. Ed.* **2021**, DOI: 10.1002/ange.202113135.
(34) Han, A.; Wang, X.; Tang, K.; Zhang, Z.; Ye, C.; Kong, K.; Hu, H.; Zheng, L.; Jiang, P.; Zhao, C., An Adjacent Atomic Platinum Site Enables Single - Atom Iron with High Oxygen Reduction Reaction Performance. *Angew. Chem. Int. Ed.* **2021**, *60*, 19262-19271.
(35) Lei, Y.; Butler, D.; Lucking, M. C.; Zhang, F.; Xia, T.; Fujisawa, K.; Granzier-Nakajima, T.; Cruz-Silva, R.; Endo, M.; Terrones, H., Single-atom doping of MoS_2 with manganese enables ultrasensitive detection of dopamine: Experimental and computational approach. *Sci. Adv.* **2020**, *6*, eabc4250.
(36) Ouyang, W.; Zeng, D.; Yu, X.; Xie, F.; Zhang, W.; Chen, J.; Yan, J.; Xie, F.; Wang, L.; Meng, H., Exploring the active sites of nitrogen-doped graphene as catalysts for the oxygen reduction reaction.*Int. J. Hydrog. Energy* **2014**, *39*, 15996-16005.
(37) Zhu, L.; Ong, W. L.; Lu, X.; Zeng, K.; Fan, H. J.; Ho, G. W., Substrate - Friendly Growth of Large - Sized $Ni(OH)_2$ Nanosheets for Flexible Electrochromic Films. *Small* **2017**, *13*, 1700084.
(38) Xing, Y.; Ku, J.; Fu, W.; Wang, L.; Chen, H., Inductive effect between atomically dispersed iridium and transition-metal hydroxide nanosheets enables highly efficient oxygen evolution reaction. *Chem. Eng. J.* **2020**, *395*, 125149.
(39) Guo, S.; Zhang, C.; Yang, M.; Zhou, Y.; Bi, C.; Lv, Q.; Ma, N., A facile and sensitive electrochemical sensor for non-enzymatic glucose detection based on three-dimensional flexible polyurethane sponge decorated with nickel hydroxide. *Anal. Chim. Acta* **2020**, *1109*, 130-139.
(40) Sun, X.; Du, Y.; Zhang, L.; Dong, S.; Wang, E., Luminescent supramolecular microstructures containing Ru (bpy) 32+: solution-based self-assembly preparation and solid-state electrochemiluminescence detection application. *Anal. Chem.* **2007**, *79*, 2588-2592.
(41) Yan, J.; Kong, L.; Ji, Y.; White, J.; Li, Y.; Zhang, J.; An, P.; Liu, S.; Lee, S.-T.; Ma, T., Single atom tungsten doped ultrathin alpha-$Ni(OH)_2$ for enhanced electrocatalytic water oxidation. *Nat. Commun.* **2019**, *10*, 1-10.
(42) Yang, J.; Cho, M.; Lee, Y., Synthesis of hierarchical $NiCo_2O_4$ hollow nanorods via sacrificial-template accelerate hydrolysis for electrochemical glucose oxidation. *Biosens. Bioelectron.* **2016**, *75*, 15-22.

(43) Lin, S.; Feng, W.; Miao, X.; Zhang, X.; Chen, S.; Chen, Y.; Wang, W.; Zhang, Y., A flexible and highly sensitive nonenzymatic glucose sensor based on DVD-laser scribed graphene substrate. *Biosens. Bioelectron.* **2018**, *110*, 89-96.
(44) Naik, K. K.; Gangan, A.; Chakraborty, B.; Nayak, S. K.; Rout, C. S., Enhanced Nonenzymatic Glucose-Sensing Properties of Electrodeposited $NiCo_2O_4$-Pd Nanosheets: Experimental and DFT Investigations. *ACS Appl. Mater. Interfaces* **2017**, *9*, 23894-23903.
(45) Ponnusamy, R.; Chakraborty, B.; Rout, C. S., Pd-Doped WO_3 Nanostructures as Potential Glucose Sensor with Insight from Electronic Structure Simulations. *J. Phys. Chem. B* **2018**, *122*, 2737-2746.

Table of Content